Sustainable Environment Research

RESEARCH

Open Access

Labile graphitic monolayers as a partition phase for containment of organic chemicals by graphene-based nanomaterials

Jui-Te Chen[1], Wen-Che Hou[1], Tsair-Fuh Lin[1*] and Cary T. Chiou[1*]

Abstract

Graphene-based nanomaterials (GBNMs) (e.g., graphene oxides and carbon nanotubes) display superior electronic and thermal conductivities and varying abilities to contain organic substances. This study sheds light to the idea that GBNMs behave as a dual sorbent, rather than a sole adsorbent, to extract nonionic organic solutes from water by both (competitive) adsorption and (noncompetitive) partition because of the solute interactions with various GBNM nanostructures formed by atomically-thin graphitic monolayers. Essential solute-sorption data with three model GBNMs from this research and similar data from the literature lead to a coherent view that labile graphitic monolayers in GBNMs undergo a liquid-like motion at room temperature to retain nonionic organic solutes by partition while structurally rigid graphitic clusters behave as adsorbents. Because the partition is noncompetitive, the GBNMs possessing high levels of labile graphene layers, as reflected by high BET surface areas, are capable of sequestering vastly higher levels of multiple organic solutes (especially, those of liquids) than conventional adsorbents, e.g., activated carbon (AC). Moreover, the postulated dual functionality of GBNMs makes sense of many otherwise puzzling phenomena, such as the highly concentration-dependent solute competitive effect with certain GBNMs and highly variable "adsorbed capacities" per unit surface area for different organic solutes with a GBNM versus those by a conventional adsorbent (e.g., graphite or AC).

Keywords Activated carbon, Adsorption, Graphene, Graphite, Nanomaterial, Partition, Organic pollutants

*Correspondence:
Tsair-Fuh Lin
tflin@mail.ncku.edu.tw
Cary T. Chiou
carychio@mail.ncku.edu.tw
Full list of author information is available at the end of the article

Graphical Abstract

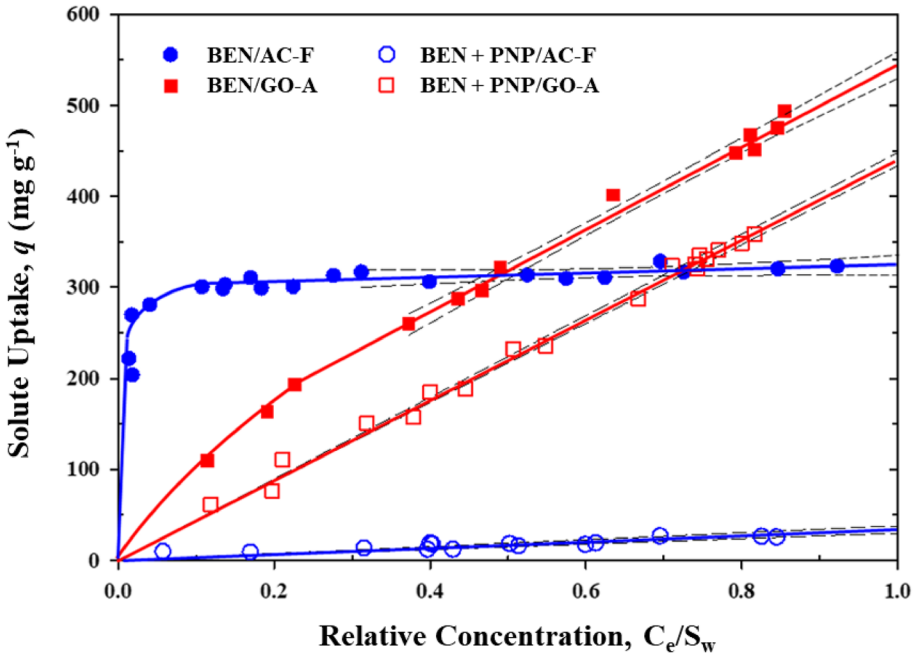

1 Introduction

As an array of sp^2 carbons fitted to 2-dimensional hexagonal lattices, graphene-based nanomaterials (GBNMs) manifest superior electronic and thermal conductivity [1, 2], exceptional mechanical strength [3], and large exposed surfaces [4, 5]. These unique features promote the use of GBNMs in electronics, photonics, and energy storage/transport [6, 7] and in the abatement of organic wastes [4, 8, 9]. For the latter objective, a number of studies have explored the efficiencies of GBNMs in different forms, e.g., graphene oxides (GO) and single-walled and multi-walled carbon nanotubes (SWCNTs; MWCNTs), to extract various organic chemicals, as summarized in recent reviews [4, 10, 11]. In these studies, the GBNMs are generally portrayed as graphite-based adsorbents, with their BET-N_2 surface areas (SAs) or pore volumes selected as basic parameters for characterizing their adsorptive potentials.

Characteristic features supporting the GBNMs as "adsorbents" to capture organic chemicals (solutes) from water include (i) an approximate linear correlation between the limiting uptakes of given solutes by GBNMs (q^o) and the BET SAs or pore volumes of the GBNMs [4, 11, 12] and (ii) a strong depression of the GBNM uptake of a target solute (e.g., naphthalene) at concentrations far below its solubility in water by other coexisting solutes (e.g., phenanthrene or pyrene) [4, 13]. Whereas the observed solute competition is illustrative of the adsorptive nature of a GBNM, the same GBNM-solute system displays a surprising additive uptake when the levels of individual co-solutes are raised close to their solubilities in water [13]. In the latter case, the total limiting q^o found for a ternary-solute system (i.e., naphthalene + phenanthrene + pyrene) with a MWCNT exceeds any single-solute q^o by more than a factor of 2. Such unusual scenarios imply that GBNMs do not perform like a conventional adsorbent.

Unlike common solid substances, GBNMs are made principally of atomically thin graphene monolayers with the end products displaying a variety of surficial structures and aggregation states, e.g., from well detached monolayers to rigidly assembled clusters. At room temperature, suspended graphene monolayers are known to exhibit out-of-plane motions due to thermal activation [14–16]. Thus, if a GBNM contains a significant fraction of such loose monolayers, the combined out-of-plane motion may produce a sizable solvent-like partition phase along with the GBNM's fixed adsorptive sites formed by rigid graphitic clusters [4, 17]. On this basis, a GBNM behaves as a dual sorbent, with the total solute uptake consisting of both adsorption and partition, with the relative magnitudes determined by specific GBNM and solute properties. The postulated dual GBNM behavior is depicted in a schematic plot of the solute uptake by

a GBNM (q) in terms of its adsorption and partition components versus the solute relative concentration (C_e/S_w) in Fig. 1, with C_e denoting the equilibrium concentration and S_w the solute water solubility. The adsorbed-solute isotherm is typically concave-downward in shape at low C_e/S_w while the partition isotherm is virtually linear over the entire range. The combined adsorption and partition uptake of a solute may be expressed as

$$q = q_{ads} + q_{par} = q_{ads} + K_p C_e \quad (1)$$

where q (g g^{-1}) is the total uptake of solute for the dual sorbent, q_{ads} is adsorption capacity (g g^{-1}), q_{par} is partition capacity (g g^{-1}), K_p is the partition coefficient ((g g^{-1}) (mL g^{-1}), C_e is the equilibrium concentration (g mL^{-1}).

Therefore, if the solute partition uptake is significant at mid to high C_e/S_w, the total solute-uptake isotherm will be practically linear at high C_e/S_w with a slope value close to that of the solute partition isotherm [18].

The truly adsorbed capacities of single organic solutes on a GBNM at given C_e/S_w are usually comparable if the solutes have similar densities, except for cases involving bulky solid adsorbates on highly porous adsorbents, e.g., activated carbon (AC), due to the molecular sieving and/or inefficient adsorbate packing [19, 20]. On the other hand, the solute partition with a GBNM should vary sensitively with the solute solubility, analogous to the solute partition to a solvent or an amorphous substance [18, 21]. The partition hypothesis for a GBNM could be best examined against the sorption data of liquid benzene (BEN) versus solid naphthalene (NPL) or phenanthrene (PHN) on a GBNM because these aromatic solutes are structurally similar to each other and to GBNMs. In this case, BEN (as a liquid) is anticipated to exhibit a sharply higher partition with a GBNM than either NPL or PHN (as a solid) because of the melting-point effect on the solute activity (a) (where $a = 1$ for a pure liquid and < 1 for a solid) [22]. Thus, if the solute adsorption and partition components with a GBNM could be decoupled by an experimental technique, as described later, the isolated partition capacities can then be tested against the calculated solute activities and the isolated adsorption capacities may be compared to each other for consistency with the expectation. To the extent that the GBNM dual functionality is satisfied, the total uptake of a liquid solute (e.g., BEN) and its isotherm slope at high C_e/S_w would be substantially higher than that of a similar but less soluble solid (e.g., PHN). Whereas this scenario has been partially realized, e.g., by the higher single-solute uptake of aniline over that of PHN or pyrene on a MWCNT [13, 23], a rigorous proof of the hypothesis demands a coherent account of other important characteristics.

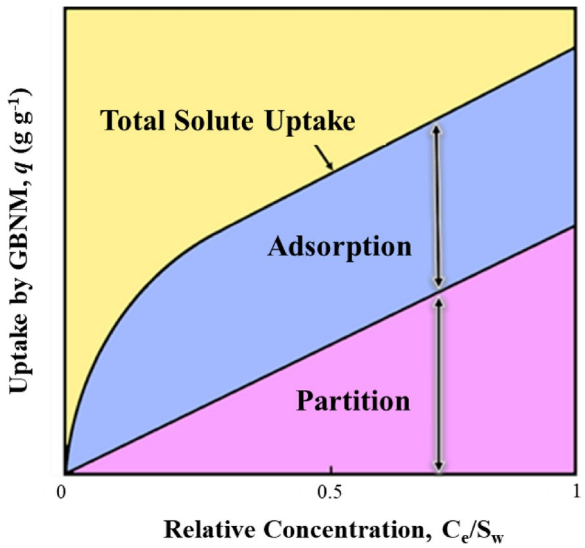

Fig. 1 Postulated dual functions of a GBNM for uptakes of organic chemicals

In this study, the sorption data of BEN, NPL, PHN, and other solutes on three GBNMs (a graphene oxide, a SWCNT, and a MWCNT) have been determined and compared with the respective adsorption data on a microporous AC and a mesoporous carbon black for testing the hypothesized GBNM dual functionality. To aid in this analysis, the total solute-uptake isotherms with these GBNMs have also been decoupled into adsorption and partition components through an adsorptive displacement method [18]. This allows for a close analysis of the solute-GBNM adsorption and partition data for their consistency with the theoretical expectation.

2 Materials and methods

2.1 Materials

Compounds employed as model organic contaminants (solutes) in sorption experiments, i.e., BEN (purity, 99.5%), NPL (99%), PHN (99%), trichloroethylene (TCE) (> 99.5%), 1,2,3-trichlorobenzene (1,2,3-TCB) (99%), 1,2,4-trichlorobenzene (1,2,4-TCB) (99%), and *p*-nitrophenol (PNP) (99%), were all purchased from Aldrich and used directly as received. The physicochemical properties of these compounds are listed in Table S1 of the Supplementary Materials (SM).

Three GBNMs along with a microporous AC (AC-F) and a mesoporous graphitized carbon black (GCB) were chosen as the model sorbents. Selected GBNMs include a graphene oxide (denoted as GO-A), a SWCNT (or CNT-S), and a MWCNT (CNT-M). GO-A was obtained from Angstron Materials Asia (Taipei, Taiwan), CNT-S from Nanostructured & Amorphous Materials (Texas, USA), and CNT-M from Nanotech Port Co. (Shenzhen, Guangdong, China). As a powder, GO-A has a reported oxygen content of ~ 20% and a dry-layer thickness of

about 2–3 nm. CNT-S contains > 95% carbon nanotubes and < 5% impurities, the latter being mainly amorphous carbon and trace metals; the nanotubes have a reported outside diameter of < 2 nm and lengths of 5–30 μm. CNT-M contains > 97% carbon nanotubes with reported outer diameters of 10 to 20 nm and lengths of 5–15 μm. All three GBNM samples were used as received for sorption experiments without further treatment. AC-F was supplied by Calgon Carbon Corporation (Pittsburgh, PA) and GCB was supplied by Sigma-Aldrich. AC-F received was milled to bulk sizes of 0.030–0.042 mm for later solute-adsorption experiments. GCB was received as a powder with a particle size of 0.237 μm and used without further treatment.

2.2 Sample characterization

Procedures for elemental (C, H, N and O) analyses, ash contents, and SAs of the selected GBNMs followed the methods described elsewhere [18]. The sample SAs, micropore volumes (V_{mic}'s), and mesopore volumes (V_{mes}'s) were all determined from the N_2-adsorption data at liquid-N_2 temperature (-196 ℃) using a Micromeritics ASAP 2020 analyzer; the SAs were calculated by the BET equation, the V_{mic}'s by the *t*-plot, and the V_{mes}'s by the BJH method. Measured SAs, pore volumes, and elemental compositions of the samples are listed in Table 1.

2.3 Sorption experiments

The solute-sorption experiments with three GBNMs, AC-F and GCB were carried out at 25 ± 1 ℃ using a batch equilibration method. The test samples were contained in 40-mL amber-glass vials, fitted with Teflon septa that were lined with aluminum foils to avoid the solute sorption by the septa. Background water solutions were prepared using deionized water containing 0.01 M $CaCl_2$ in ionic strength and 200 mg L^{-1} NaN_3 for inhibiting the microbial activity. In single-solute sorption experiments, a group of vials were filled with known levels of a GBNM, AC-F or GCB (5–400 mg) and 40 mL of the background solution with varying amounts of a solute, leaving little headspace to minimize the volatile loss. The solid-to-water ratios were adjusted such that the solute uptake reached 30–80% of the amount in the control solutions containing no sorbent. A stock solution of each target solute in methanol was used for preparing the initial solute doses in water, with the amount of methanol added to the solution kept below 0.1% in volume to minimize the co-solvent effect. Vials of prepared samples were rotated on an overturn shaker at 20 rpm for 2 d for AC-F or GCB, 3 d for GO, and 4 d for SWCNT and MWCNTs. Sorption kinetic experiments assured that solutes in solid and solution reached equilibrium at the stated equilibration times. The pH values of the samples were all maintained between 7.0 and 7.5 during the sorption experiments.

Following the equilibration, the vails were centrifuged at 3000 rpm for 30 min controlled at 25 ± 1 ℃ (Centrifuge 16R, Thermo Scientific) and aliquots of supernatants were withdrawn for solute analyses. For highly volatile BEN and TCE, supernatants (20–30 μL) were transferred directly using a microsyringe into septum-sealed vials filled with methanol to minimize the solute volatile loss for subsequent solute analyses. For other solutes, supernatants (10 mL) were removed and extracted by hexane (v/v 1:1) for solute analyses. All solute masses were analyzed by Agilent 7890A GC/MS comprised of a 5975C ion-trap MS (Agilent, USA) and a HP-5 capillary column.

The amount of a solute sorbed to a solid was calculated by mass balance, based on the measured solute level in the control (i.e., the one prefixed with a known solute level in water but no sorbent) and the detected solute level in the test sample (the one prefixed with the same initial solute level and a fixed amount of sorbent). Observed recoveries of the solutes in control samples were in the range of 92–99%; the specific value for a given solute-GBNM system was used for the mass-balance calculation.

On determining the solute partition capacities with a GBNM by using saturated PNP as the adsorptive displacer, neat PNP (with $S_w = 16$ g L^{-1}) was weighed into to the solid-water slurries at 20–24 g L^{-1}. This level was sufficient to keep water and the solid phase fully saturated with PNP without forming a large excess. To construct the sorption isotherm of a test solute, varying amounts of solutes in methanol were applied to the solid-water slurry

Table 1 Ash-free elemental compositions, ash contents, and BET-N_2 SAs of F300 activated carbon (AC-F), a graphitized carbon black (GCB), a graphene oxide (GO-A), a single-wall carbon nanotube (CNT-S), and a multi-wall carbon nanotube (CNT-M) used in this study

Materials	C (%)	H (%)	N (%)	O (%)	Ash (%)	SA[a] (m^2 g^{-1})	V_{mic}[b] (cm^3 g^{-1})	V_{mes}[c] (cm^3 g^{-1})
AC-F	89.5	1.22	0.49	8.76	7.22	801	0.35	0.19
GCB	96.7	0.16	0.59	2.54	0.79	190	0.03	0.47
GO-A	80.6	0.59	0.28	18.5	1.73	425	0.05	2.56
CNT-S	93.1	0.71	0.13	5.55	< 5[d]	423	0.008	1.29
CNT-M	99.4	0.25	0.03	0.36	0.49	110	0.01	0.62

[a] Surface area, [b]Micropore volume, [c]Mesopore volume, [d]Data from the manufacturer

with the experiments carried out using the procedure as described.

3 Results and discussion

3.1 Adsorption characteristics of solutes with and without PNP on AC-F and GCB

Before inspecting the solute sorption data on selected GBNMs, we examine first the adsorption data of BEN and PHN on AC-F (Fig. 2a and b) and similar data on GCB (Fig. 2c and d) to highlight the distinct adsorption features with the two reference adsorbents, a microporous AC-F (SA = 801 m^2 g^{-1}) and a mesoporous GCB (SA = 190 m^2 g^{-1}). The adsorption capacities and isotherm shapes with these samples serve to validate the decoupled GBNM adsorption components described later.

In Fig. 2, the solute mass adsorbed by a unit mass of AC-F or GCB (q) at 25 ± 1 ℃ is plotted versus the solute C_e/S_w. Since AC-F and GCB are pure adsorbents, the solute uptake by AC-F or GCB occurs only by adsorption. The isotherms of BEN and PHN on microporous AC-F are mutually similar in shape (i.e., sharply concave downward at low C_e/S_w) and in adsorbed capacity, especially in volume adsorbed calculated by using the pure-solute density as approximation [20]. While the respective isotherms on GCB also exhibit a similar shape and similar adsorbed volumes, they display a distinctly lower curvature at low C_e/S_w compared to that with AC-F, a characteristic of adsorption on relatively open (mesoporous) surfaces. Whereas the limiting adsorbed capacity (q^o) is clearly higher on AC-F because of the higher SA, the limiting capacities per unit SA (i.e., q^o/SA) for the solutes with GCB are somewhat higher, a result possibly related to the lower oxygen content of GCB (see Table 1).

Also included in Fig. 2 are the isotherms of solutes adsorbed on AC-F and GCB when saturated PNP, the adsorptive displacer, is added to displace the adsorbed target solutes. With PNP added, the initially marked solute uptakes and nonlinear isotherm shapes are drastically reduced to weak linear uptakes, with the residual (unsuppressed) adsorbed capacities < 5–10% of the single-solute values at $C_e/S_w \leq 0.9$. These results are in

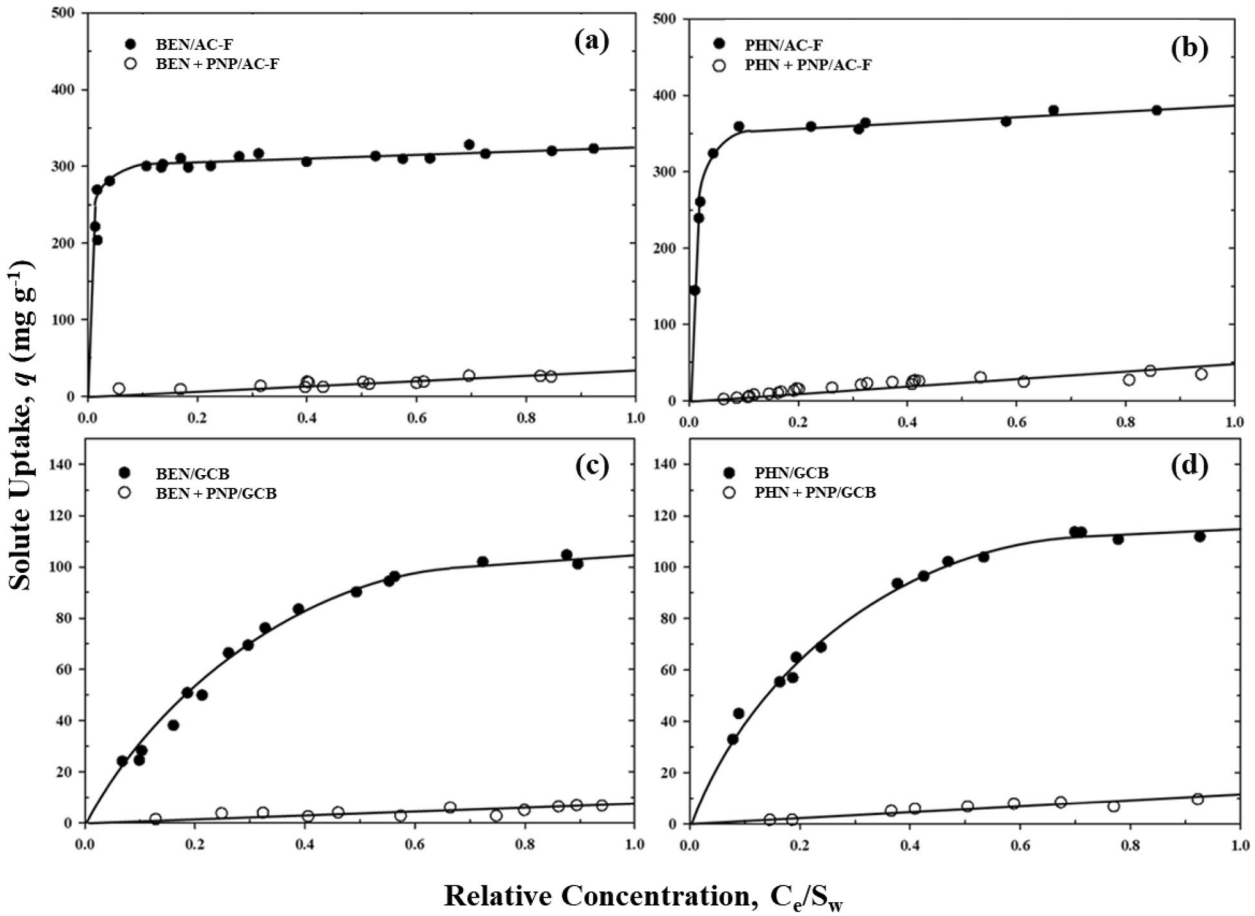

Fig. 2 Sorption of BEN and PHN from water with and without saturated PNP on AC-F (**a**, **b**) and a graphitized carbon black (GCB) (**c**, **d**) at 25 ± 1 ℃

sharp contrast to the organic-solute partition to a non-porous amorphous organic matter (e.g., the soil organic matter), where the solute uptake isotherm is linear [24, 25] and not interfered by PNP or other solutes [18, 21]. As such, PNP serves as a powerful adsorptive displacer for estimating the solute adsorption capacity (based on the extent of solute displaced) without affecting the solute partition when the total solute uptake by a sorbent involves both adsorption and partition.

3.2 Decoupled solute-GBNM adsorption and partition characteristics

To examine the postulated dual function of a GBNM, we start by comparing the sorption isotherms of BEN and PHN from water on GO-A in Fig. 3 with those on AC-F and GCB in Fig. 2. The BET SA of GO-A is 425 m^2 g^{-1} versus 801 m^2 g^{-1} for AC-F and 190 m^2 g^{-1} for GCB. As seen, the BEN and PHN isotherms on GO-A differ widely from those on AC-F in shape and capacity. For instance, at low C_e/S_w (≤ 0.2), the BEN uptake by AC-F is vastly higher than that by GO-A; however, at $C_e/S_w \geq 0.6$, the opposite occurs, with the limiting BEN capacity (i.e., q^o) being about 325 mg g^{-1} on AC-F and 540 mg g^{-1} on GO-A despite that GO-A has a SA only about one half that of AC-F. Similarly, although the BEN isotherm on GO-A is quite similar in shape to that on GCB because of their mesoporous structures, the limiting q^o on GO-A is > 5 times that on GCB, whereas the SAs of GO-A and GCB differ only by about a factor of 2. These findings strongly imply that the uptake of BEN and other organic solutes by GO-A proceeds by more than just a simple adsorption process.

On the premise that GBNMs perform as a dual-function sorbent, the partition capacities of different solutes with a GBNM are anticipated to vary sensitively with their solubilities in a solvent or an amorphous substance while the respective adsorption capacities should be fairly comparable. The uptake isotherms of BEN, NPL, PHN, and TCE on GO-A with and without PNP as the adsorptive displacer are shown in Fig. 3 for inspection. Here the total uptake capacities at $C_e/S_w = 1$ increase sharply from about 215 mg g^{-1} for PHN, 260 mg g^{-1} for NPL to

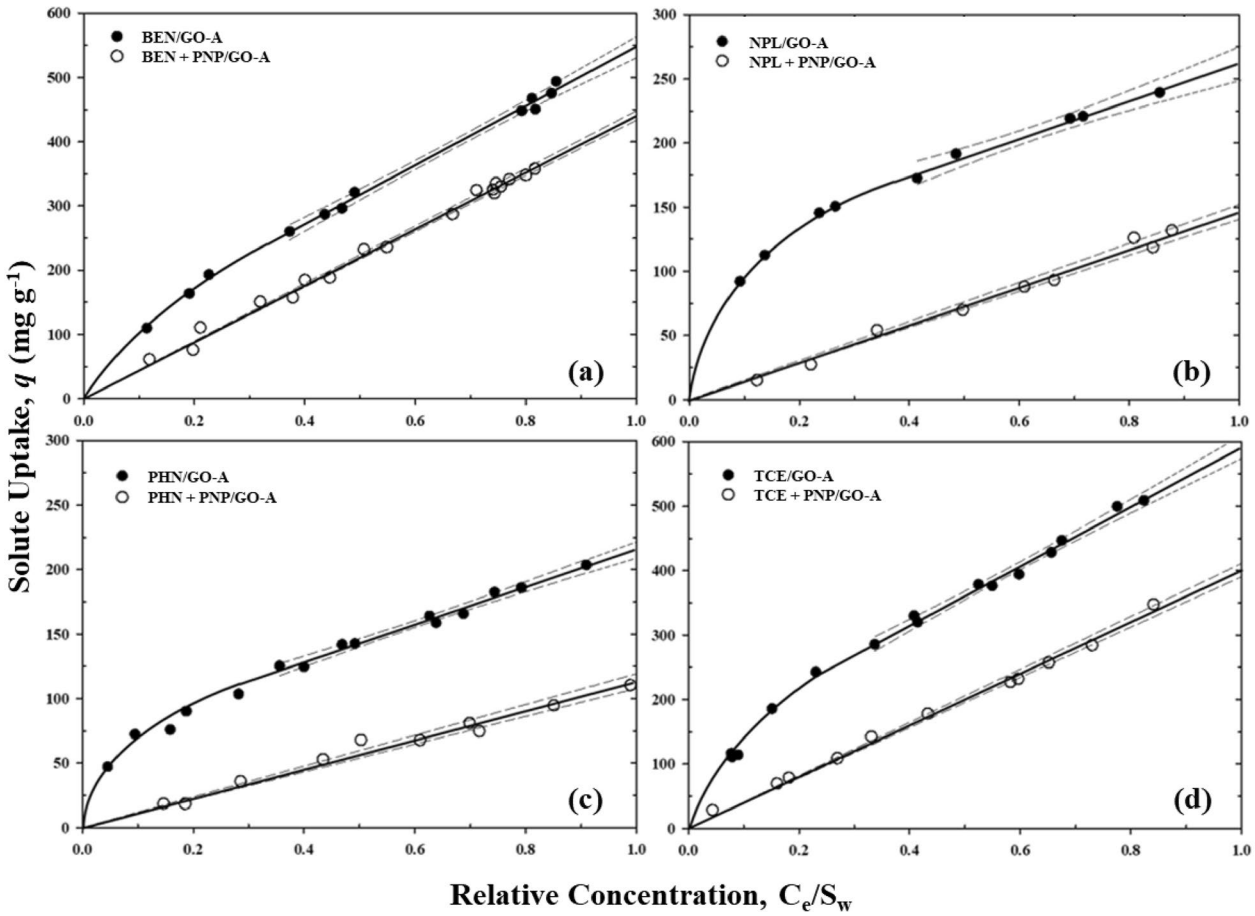

Fig. 3 Sorption of (**a**) BEN, (**b**) NPL, (**c**) PHN, and (**d**) TCE from water with and without saturated PNP on a graphene oxide (GO-A) at 25 ± 1 ℃, where the dashed lines represent ± 95% confidence intervals

540 mg g^{-1} for BEN. The linear isotherms with different slopes derived from the PNP addition express to a good approximation the respective solute partition capacities (q_{par}) in view of the sharp adsorptive depression on AC-F and GCB by added PNP. Hence, the difference between q and q_{par} at a C_e/S_w gives a logical estimate of the solute adsorption capacity (q_{ads}). In this account, the small residual linear solute adsorption with added PNP could be neglected for simplicity unless the resolved adsorption component is very small. In Fig. 3, the shapes of isolated adsorption isotherms with GO-A resemble closely those with GCB in reflection of their mesoporous structures. The limiting q^o_{ads}'s and q^o_{par}'s of solutes at $C_e/S_w = 1$ are listed in Table 2.

The q^o_{ads}'s and q^o_{par}'s in mL g^{-1} listed in Table 2 are obtained from the respective values in mg g^{-1} using the pure-solute densities. As seen, the limiting q^o_{ads}'s (mL g^{-1}) for these solutes are fairly constant while the respective q^o_{par}'s (mL g^{-1}) form a distinct order BEN > NPL > PHN, with the q^o_{par} of BEN being about 3.9 times that of NPL and 5.5 times that of PHN. These q^o_{par}'s (mL g^{-1}) are closely linearly related to the pure-solute activities, i.e., 1 for liquid BEN, about 0.30 for solid NPL, and 0.22 for solid PHN at 25 ℃; the solid activities are calculated from their melting points and molar heats of fusion (see Table S1) using the standard thermodynamic equation [22]. As shown later, this distinct relation between q^o_{par}'s (mL g^{-1}) and solute activities is well conserved with two other model GBNMs, a SWCNT and a MWCNT. For BEN, NPL, and PHN, the noted correlation of solute q^o_{par}'s with activities is well in line with the fact that the activity of a solute in solution is equal to the solute volume (or mole) fraction times the solute activity coefficient [22]. For homologs of chemicals in a narrow series (e.g., BEN, NPL, and PHN), the activity coefficients in an organic solvent are either fairly constant or increase to a small-to-moderate extent with increasing molecular weight. The solute q^o_{par}'s (mL g^{-1}) with a GBNM should thus be largely proportional to the solute volume-fraction solubilities or the pure-solute activities. For solutes from mixed classes, this correlation may become less distinct because of the increasingly disparate solute activity coefficients.

Also included in Fig. 3 and Table 2 for comparison are the q^o_{ads} and q^o_{par} of liquid TCE on GO-A. Here the TCE q^o_{ads} (mL g^{-1}) is close to that of BEN while the q^o_{par} (mL g^{-1}) is about one half that of BEN. These results appear to make good sense because TCE with a considerably higher density than that of BEN (see Table S1) should register a higher q^o_{ads} in mg g^{-1} but a similar q^o_{ads} in mL g^{-1} while BEN with an expectedly higher compatibility than TCE with the GO-A's liquid-like phase should register a higher q^o_{par} (mL g^{-1}). The slightly higher q^o_{ads}'s (mL g^{-1}) of liquid BEN and TCE than those of solid NPL and PHN reflect possibly an improved packing of the condensed liquids over that of the condensed solids on GO-A. On the other hand, the intimate correlation between the q^o_{par}'s (mL g^{-1}) and activities of BEN, NPL, and PHN (Table 2) is well consistent with the finding that the solute activity in a solution is best accounted for by the solute volume fraction [22, 26]. The results suggest that BEN, NPL, and PHN as dissolved solutes exhibit about the same compatibility (or activity coefficient) with the GO-A's liquid-like phase, which seems very reasonable.

From the above analysis, one also expects the sorption capacities of 1,2,4-TCB and 1,2,3-TCB on a GBNM to be distinctly different. At room temperature, 1,2,4-TCB is a liquid while 1,2,3-TCB is a solid with a melting point of 53 ℃; the two isomers have nearly the same densities. The activity of liquid 1,2,4-TCB is 1 and that of 1,2,3-TCB about 0.55 based on its melting point and molar heat of fusion (Table S1). Since the two isomeric

Table 2 Pure-solute activities at 25 ℃ (a), limiting adsorption capacities (q^o_{ads}), and limiting partition capacities (q^o_{par}) of organic compounds from water on GO-A at room temperature (25 ± 1 ℃). The CI inside parentheses refers to the 95% confidence interval

Compound	a[a]	q^o_{ads} (± CI)[b] (mg g^{-1})	q^o_{ads} (± CI)[b] (mL g^{-1})	q^o_{par} (± CI) (mg g^{-1})	q^o_{par} (± CI) (mL g^{-1})
BEN	1	100 (± 22)	0.11 (± 0.03)	440 (± 8)	0.50 (± 0.009)
NPL	0.30	110 (± 20)	0.097 (± 0.02)	150 (± 8)	0.13 (± 0.007)
PHN	0.22	110 (± 10)	0.093 (± 0.008)	110 (± 6)	0.089 (± 0.005)
TCE	1	180 (± 28)	0.12 (± 0.02)	400 (± 11)	0.27 (± 0.008)
1,2,3-TCB	0.55	160 (± 16)	0.11 (± 0.01)	140 (± 4)	0.093 (± 0.003)
1,2,4-TCB	1	180 (± 22)	0.12 (± 0.02)	280 (± 8)	0.19 (± 0.006)

[a] The activity of a solid compound at 25 ℃ is calculated from the compound's melting temperature and molar heat of fusion listed in Table S1 using the standard thermodynamic equation, i.e., $\ln a = (-\Delta\overline{H}_f/R)(T_m - T)/TT_m$, where $\Delta\overline{H}_f$ is the molar heat of fusion, R is the gas constant, T_m is the melting point (K), and T is the system temperature (K)

[b] The 95% CI's of q^o_{ads}'s are based on the 95% CI's of the q^o and q^o_{par} data, where $q^o_{ads} = q^o - q^o_{par}$; the 95% CI's of the q^o's are based on the upper linear sections of the single-solute isotherms

solutes should have about the same compatibility (or activity coefficient) in a solution phase, liquid 1,2,4-TCB should exhibit a q^{o}_{par} about twice that of solid 1,2,3-TCB while their q^{o}_{ads}'s be about the same. Measured sorption isotherms of the two solutes with and without PNP on GO-A in Fig. S1 (SM) give q^{o}_{par} = 135 mg g^{-1} (or 0.0931 mL g^{-1}) and q^{o}_{ads} = 160 mg g^{-1} (or 0.110 mL g^{-1}) for 1,2,3-TCB and q^{o}_{par} = 275 mg g^{-1} (or 0.190 mL g^{-1}) and q^{o}_{ads} = 180 mg g^{-1} (or 0.124 mL g^{-1}) for 1,2,4-TCB (see Table 2). The data agree well with the prediction. Note also that the q^{o}_{ads}'s (mL g^{-1}) of 1,2,3-TCB and 1,2,4-TCB agree well with the q^{o}_{ads}'s (mL g^{-1}) of other solutes in Table 2.

We consider next the uptake capacities of the same solutes (BEN, NPL, PHN, and TCE) on CNT-S, a SWCNT, that has a SA (423 m^2 g^{-1}) basically the same as that of GO-A (425 m^2 g^{-1}) and on CNT-M, a MWCNT, that has a much smaller SA (110 m^2 g^{-1}). The solute isotherms with and without PNP (as the adsorptive displacer) on CNT-S are displayed in Fig. 4 and the resolved q^{o}_{ads}'s and q^{o}_{par}'s listed in Table 3; the similar isotherms and q^{o}_{ads}'s and q^{o}_{par}'s with CNT-M are given in Fig. S2 (SM) and Table 3. As seen, the major sorption characteristics with these two GBNMs are remarkably the same as with GO-A, i.e., the solute q^{o}_{par}'s mL g^{-1}) are intimately related to the solute activities and the individual solute q^{o}_{ads}'s (mL g^{-1}) with either GBNM are similar despite that the solute q^{o}_{par}'s or q^{o}_{ads}'s with the two GBNMs are very different. On CNT-S, the solute q^{o}_{ads} is about 40–50% higher than with GO-A while the solute q^{o}_{par} is only about half that with GO-A. On CNT-M, the q^{o}_{ads} is about 5 times smaller than that of GO-A and the q^{o}_{par} is 7–7.5 times smaller than that of GO-A. As explained later, the large disparities in solute q^{o}_{ads}'s and q^{o}_{par}'s with GO-A and CNT-M result mainly from markedly different SAs of the samples that impact the solute adsorption and partition. The opposite trends exhibited by the solute q^{o}_{ads}'s and q^{o}_{par}'s with GO-A and CNT-S, which have essentially equal SAs, imply that there are relatively fewer labile graphene monolayers in aqueous CNT-S systems than needed to form as effective a partition phase as that in GO-A at room temperature.

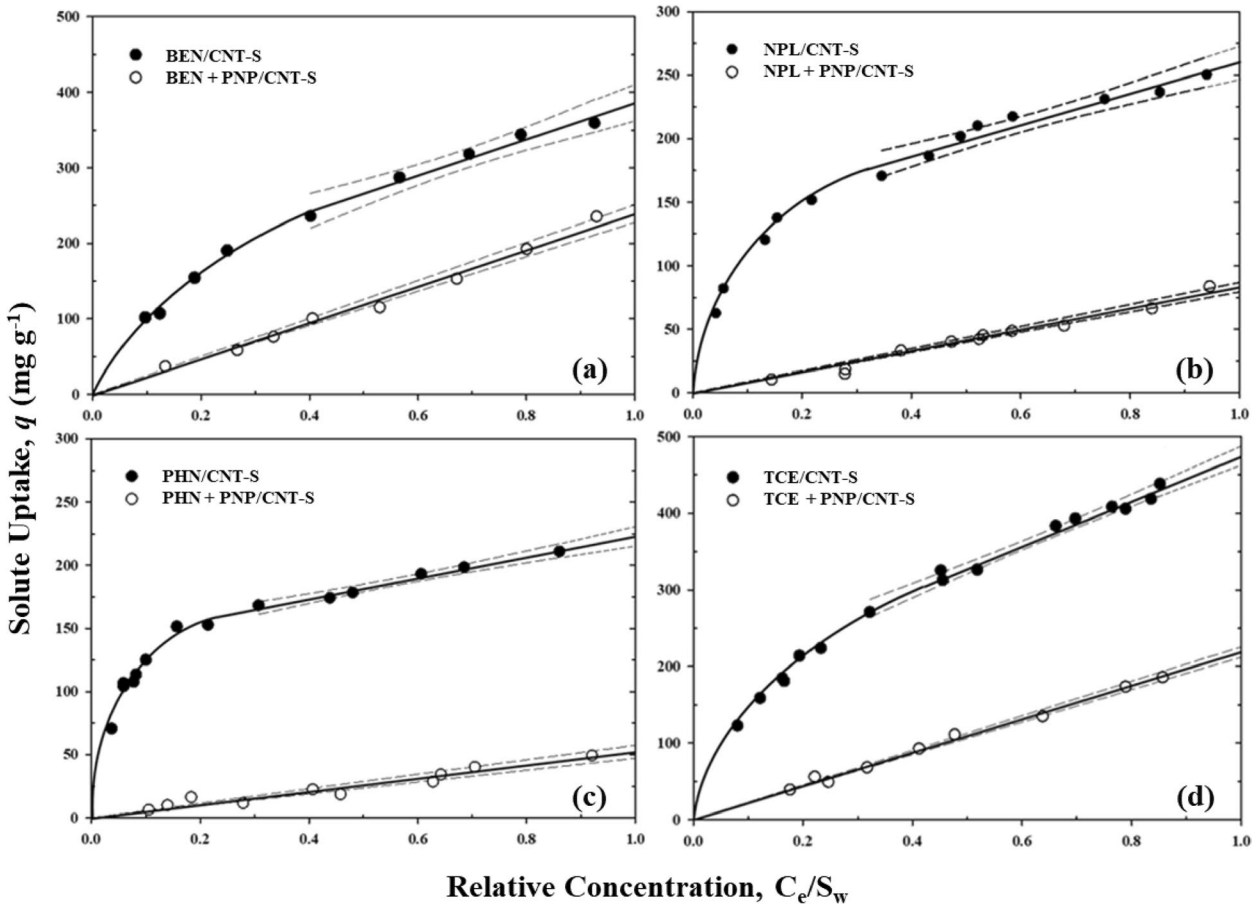

Fig. 4 Sorption of (**a**) BEN, (**b**) NPL, (**c**) PHN, and (**d**) TCE from water with and without saturated PNP on a single-walled carbon nanotube (CNT-S) at 25 ± 1 ℃, where the dashed lines represent ± 95% confidence intervals

Table 3 Limiting adsorption capacities (q^{o}_{ads}) and limiting partition capacities (q^{o}_{par}) of BEN, NPL, PHN, and TCE from water on CNT-S and CNT-M at room temperature (25 ± 1 ℃). The CI inside parentheses refers to the 95% confidence interval

Compound	q^{o}_{ads} (±CI)[a] (mg g^{-1})	q^{o}_{ads} (±CI)[a] (mL g^{-1})	q^{o}_{par} (±CI) (mg g^{-1})	q^{o}_{par} (±CI) (mL g^{-1})
CNT-S				
BEN	145 (±32)	0.166 (±0.04)	240 (±12)	0.274 (±0.001)
NPL	180 (±15)	0.157 (±0.01)	80 (±4)	0.0701 (±0.004)
PHN	175 (±15)	0.148 (±0.01)	50 (±5)	0.0424 (±0.004)
TCE	265 (±20)	0.182 (±0.01)	215 (±7)	0.147 (±0.005)
CNT-M				
BEN	17 (±3)	0.019 (±0.003)	61 (±1)	0.070 (±0.001)
NPL	18 (±3)	0.016 (±0.003)	17 (±0.5)	0.015 (±0.0004)
PHN	21 (±4)	0.018 (±0.003)	14 (±0.5)	0.012 (±0.0004)
TCE	29 (±5)	0.020 (±0.003)	60 (±2)	0.041 (±0.001)

[a] The 95% CI's of q^{o}_{ads}'s are based on the 95% CI's of the q^{o} and q^{o}_{par} data, where $q^{o}_{ads} = q^{o} - q^{o}_{par}$; the 95% CI's of the q^{o}'s are based on the upper linear sections of the single-solute isotherms

3.3 Correlations of current findings with literature reports

With the similar q^{o}_{ads}'s (mL g^{-1}) of BEN, NPL, PHN, and TCE on each of the three model GBNMs, the total solute uptakes (q^{o}'s) in mL g^{-1} on a GBNM line up in the same order BEN > TCE > NPL > PHN as that for the solute q^{o}_{par}'s (mL g^{-1}). This discloses that the solute partition contribution is mainly responsible for the different solute q^{o}'s (mL g^{-1}) with a GBNM. In earlier studies of the uptakes of liquid aniline versus other solid solutes by a MWCNT, Yang et al. [23] found that the observed q^{o}'s (mL kg^{-1}) fall in the order aniline > NPL > PHN > pyrene, which is exactly that of the pure-solute activities. Thus, the combined data of this study and Yang et al. [23] clearly illustrate that a GBNM can withhold a considerably greater quantity of relatively soluble liquid compounds than that of similar but less soluble solid compounds because of the enhanced liquid partition. This view is keenly consistent with the compiled data of various liquid and solid organic compounds with a number of GBNMs examined [4].

Because of the noncompetitive nature of a partition process, a GBNM with a large partition domain could thus withhold an exceptionally large quantity of many coexisting solutes combined, especially those of liquids, at high C_e/S_w. To highlight this effect, the observed total uptake of BEN at $C_e/S_w = 0.92 \pm 0.08$ and TCE at $C_e/S_w = 0.92 \pm 0.01$ as binary solutes on GO-A in two experiments yield $q = 908 \pm 11$ mg g^{-1}, namely 458 ± 4 mg g^{-1} for BEN and 450 ± 7 mg g^{-1} for TCE. Here the individual BEN or TCE uptake is greater than its partition level but less than its total uptake at the stated C_e/S_w, which is illustrative of the noncompetitive solute partition and competitive solute adsorption. The huge BEN + TCE capacity on GO-A exceeds any known limiting capacities of organic solutes adsorbed by conventional ACs [20]. Clearly, without the concurrent solute partition, no pure adsorbents could ever achieve this exceptional large capacity either for single solutes or for many solutes combined. The above analysis also makes sense of the unusual finding by Yang et al. [13] that the total uptake (> 150 mg g^{-1}) of coexisting NPL, PHN, and pyrene at near their saturation levels in water by a MWCNT (SA = 174 m^2 g^{-1}) is more than twice the limiting capacity of any solute alone (42–74 mg g^{-1}).

In principle, the additive uptakes of multiple solutes at high C_e/S_w by certain GBNMs would diminish at small C_e/S_w, due not only to the reduced solute level but also to the faster decline of the linear solute partition than the nonlinear solute adsorption. That is, as the C_e/S_w decreases, a GBNM becomes increasingly like a conventional adsorbent such that the system exhibits a much sharper solute competitive effect, as noted by Yang et al. [13] in studies of the NPL sorption at low C_e/S_w with PHN and pyrene as co-solutes by the same MWCNT as indicated before. Another case where a strong solute competition for a GBNM is anticipated is that of a multisolute system comprised of highly insoluble organic solutes, typically solid compounds with very high melting points. Relevant data on this issue await to be provided. Apparently, the postulated partition effect for a GBNM as evidenced by the data in this study also occurs to other GBNMs, although the extent varies with the system.

It is noted with interest that the limiting solute adsorbed per unit SA (q^{o}_{ads}/SA) with certain GBNMs are considerably smaller than those with conventional graphitized adsorbents (e.g., AC or GCB). For instance, BEN exhibits a q^{o}_{ads}/SA of 0.24 mg m^{-2} on GO-A, 0.34 mg m^{-2} on CNT-S, 0.41 mg m^{-2} on AC-F, and 0.53 mg m^{-2} on GCB. The sharply lower value with GO-A appears to result in part from the transition of a significant amount of labile graphitic monolayers to a liquid-like phase at room temperature. This effect is apparently less significant with CNT-S due presumably to its more rigid nano-wall graphitic structure. Keep in mind that the SAs of solids are customarily measured using the N_2 adsorption data at the liquid N_2 temperature (77 K). At such a low temperature, all GBNM components are under a rigid frozen state and all exposed surfaces are detected. The GBNM SAs detected consist primarily of relatively open graphitic surfaces [27–29], as listed in Table 1, rather than from fine pores or slits (0.3–2.0 nm in width), which also agrees with the noted low isotherm curvatures at low C_e/S_w for solutes on GCB and GBNMs (Figs. 2, 3 and 4 and Figs. S1 and S2). Another potential cause for lower q^{o}_{ads}/SA with GBNMs is that the London attractive forces from the

atoms of (immobile) graphitic monolayers would be weaker than the forces from surfaces of a thicker adsorbent, such as AC or GCB. However, this reduction in attractive energy is likely no more than 12–15%, considering that the London force decreases with distance by the third power [20].

Because of the transition of labile graphene layers to a partition phase at room temperature, the effective adsorptive surfaces of many GBNMs in water may be significantly less than suggested by the BET SAs of dry GBNMs at 77 K. Whereas this transition reduces the solute uptake by adsorption, it promotes the uptake by partition. As the BET SA of a GBNM would be sensitively influenced by the content of those labile graphitic layers, both the adsorption and partition uptakes of a solute by a GBNM might be linearly related to the BET SA of the GBNM if these labile layers make up a significant fraction of the GBNM mass in water. This standpoint is keenly compatible with the finding that the total (undivided) uptake capacities of given solutes (e.g., NPL) on a wide variety of GBNMs correlate to a good extent with the BET SAs of the GBNMs tested [4].

There have been attempts to evaluate the "adsorptive strengths" of various GBNMs against that of a reference carbon adsorbent (e.g., a graphite or an AC) in terms of the solute mass sorbed by a unit SA (i.e., q/SA) at a fixed solute C_e [29, 30]. Since $q = q_{ads} + q_{par}$ (Eq. 1) for solutes on GBNMs, this comparison would lead to disparate results, depending on the solute species and the C_e/S_w examined. For example, the q/SA of liquid BEN or chlorobenzene with a MWCNT (SA = 148 m^2 g^{-1}) is found to be much greater than that with a graphite (SA = 4.5 m^2 g^{-1}) at mid to high C_e/S_w but the trend is reversed at low C_e/S_w; on the other hand, the q/SA of 1,2,4,5-tetrachlorobenzene, a relatively insoluble solid, is higher on the graphite than on the same MWCNT at nearly all C_e/S_w [30]. These puzzling phenomena may now be reconciled by the dual-sorption process of GBNMs, in which the solute partition capacity varies sensitively with the GBNM structure, the solute solubility, and the C_e/S_w range analyzed, as illustrated by the current data of BEN, TCE, PHN, and other solutes. Normalization of total solute uptakes by respective SAs thus yields inconsistent results for different solutes on a GBNM or for same solutes on a GBNM against a traditional carbon adsorbent. Should the SA normalization be restricted to adsorbed fractions of the GBNM uptakes, no such large irregularities would occur, even though the q_{ads}/SA values with certain GBNMs may be significantly less than the corresponding values with conventional adsorbents.

In conclusion, the extensive organic-solute sorption data examined are keenly consistent with the suggested GBNM dual functionality, in which both the adsorption and partition domains consist of the same graphitic material while their different modes of action depend on specific nanostructures formed. Because of the strong solubility dependence of the solute partition and of the comparable adsorbed volumes between solutes, differences in total capacities of solutes sorbed by a GBNM at a fixed C_e/S_w reflect primarily the unequal solute partition contribution. With independent solute partition, GBNMs possessing large adsorption and partition domains become "a super sorbent" for relatively soluble organic chemicals. Considering the influence of complex graphitic nanostructures on the GBNM behavior, characterization of the adsorption and partition domains of a GBNM by use of appropriate reference solutes via the PNP displacement method provides a beneficial lead in assessing the capabilities of various GBNMs for abating specific organic contaminants. However, to provide additional evidence supporting the existence of the labile layer of GBNM, it is suggested that a tool capable of quantifying the labile layer based on sorbent properties be developed.

Supplementary Information

The online version contains supplementary material available at https://doi.org/10.1186/s42834-023-00197-4.

Additional file 1: Table S1. Physicochemical properties of the organic compounds selected for analysis of the GBNM sorption characteristics. **Fig. S1.** Sorption of (a) 1,2,3-TCB and (b) 1,2,4-TCB from water with and without PNP on a graphene oxide (GO-A) at 25±1 ℃, where the dashed lines represent ±95% confidence intervals. **Fig. S2.** Sorption of (a) BEN, (b) NPL, (c) PHN, and (d) TCE from water with and without saturated PNP on a multi-walled carbon nanotube (CNT-M) at 25±1 ℃, where the dashed lines represent ±95% confidence intervals.

Acknowledgements
This research is supported by Taiwan Ministry of Science and Technology (Number: MOST 106-2221-E-006-013-MY3 and MOST 107-2628-E-006-001-MY3) and National Cheng Kung University, Taiwan (the University Advancement Project sponsored by the Taiwan Ministry of Education).

Authors' contributions
This study was initiated by Cary T. Chiou, with the experiments designed and data interpreted by Cary T. Chiou, Tsair-Fuh Lin, and Wen-Che Hou, and experiments conducted by Jui-Te Chen. The manuscript was prepared by Jui-Te Chen and Cary Chiou, and modified by Tsair-Fuh Lin and Wen-Che Hou.

Funding
The study received financial support from Taiwan Ministry of Science and Technology (Grant Number: MOST 106–2221-E-006–013-MY3 and MOST 107–2628-E-006–001-MY3) and National Cheng Kung University, Taiwan (the University Advancement Project sponsored by the Taiwan Ministry of Education).

Availability of data and materials
Upon reasonable request, the corresponding author can provide access to the data produced in this study.

Declarations

Competing interests

The authors state that there are no apparent financial interests or personal relationships that could have influenced the findings presented in this paper.

Author details

[1]Department of Environmental Engineering, National Cheng Kung University, Tainan 70701, Taiwan.

Received: 2 May 2023 Accepted: 16 October 2023
Published online: 10 November 2023

References

1. Geim AK. Graphene: status and prospects. Science. 2009;324:1530–4.
2. Balandin AA. Thermal properties of graphene and nanostructured carbon materials. Nat Mater. 2011;10:569–81.
3. Lee C, Wei X, Kysar JW, Hone J. Measurement of the elastic properties and intrinsic strength of monolayer graphene. Science. 2008;321:385–8.
4. Yang K, Xing B. Adsorption of organic compounds by carbon nanomaterials in aqueous phase: Polanyi theory and its application. Chem Rev. 2010;110:5989–6008.
5. Zhu Y, Murali S, Cai W, Li X, Suk JW, Potts JR, et al. Graphene and graphene oxide: synthesis, properties, and applications. Adv Mater. 2010;22:3906–24.
6. Baughman RH, Zakhidov AA, de Heer WA. Carbon nanotubes—the route toward applications. Science. 2002;297:787–92.
7. Novoselov KS, Geim AK, Morozov SV, Jiang D, Zhang Y, Dubonos SV, et al. Electric field effect in atomically thin carbon films. Science. 2004;306:666–9.
8. Kemp KC, Seema H, Saleh M, Le NH, Mahesh K, Chandra V, et al. Environmental applications using graphene composites: water remediation and gas adsorption. Nanoscale. 2013;5:3149–71.
9. Wang X, Liu Y, Tao S, Xing B. Relative importance of multiple mechanisms in sorption of organic compounds by multiwalled carbon nanotubes. Carbon. 2010;48:3721–8.
10. Chen X, Chen B. Macroscopic and spectroscopic investigations of the adsorption of nitroaromatic compounds on graphene oxide, reduced graphene oxide, and graphene nanosheets. Environ Sci Technol. 2015;49:6181–9.
11. Apul OG, Karanfil T. Adsorption of synthetic organic contaminants by carbon nanotubes: A critical review. Water Res. 2015;68:34–55.
12. Yang K, Zhu L, Xing B. Adsorption of polycyclic aromatic hydrocarbons by carbon nanomaterials. Environ Sci Technol. 2006;40:1855–61.
13. Yang K, Wang X, Zhu L, Xing B. Competitive sorption of pyrene, phenanthrene, and naphthalene on multiwalled carbon nanotubes. Environ Sci Technol. 2006;40:5804–10.
14. Meyer JC, Geim AK, Katsnelson MI, Novoselov KS, Booth TJ, Roth S. The structure of suspended graphene sheets. Nature. 2007;446:60–3.
15. Korznikova EA, Dmitriev SV. Moving wrinklon in graphene nanoribbons. J Phys D Appl Phys. 2014;47:345307.
16. Dai C, Guo Z, Zhang H, Chang T. A nanoscale linear-to-linear motion converter of graphene. Nanoscale. 2016;8:14406–10.
17. Li XL, Wang XR, Zhang L, Lee SW, Dai HJ. Chemically derived, ultrasmooth graphene nanoribbon semiconductors. Science. 2008;319:1229–32.
18. Chiou CT, Cheng J, Hung WN, Chen B, Lin TF. Resolution of adsorption and partition components of organic compounds on black carbons. Environ Sci Technol. 2015;49:9116–23.
19. Chiou CTT, Manes M. Application of the Polanyi adsorption potential theory to adsorption from solution on activated carbon. IV. Steric factors, as illustrated by the adsorption of planar and octahedral metal acetylacetonates. J Phys Chem. 1973;77:6, 809–13. https://pubs.acs.org/doi/10.1021/j100625a015.
20. Manes M. Activated carbon adsorption fundamentals. In: Meyers RA, editor. Encyclopedia of Environmental Analysis and Remediation. New York: John Wiley & Sons; 1998, p. 26–68.
21. Chiou CT, Porter PE, Schmedding DW. Partition equilibriums of nonionic organic compounds between soil organic matter and water. Environ Sci Technol. 1983;17:227–31.
22. Chiou CT, Schmedding DW, Manes M. Improved prediction of octanol—water partition coefficients from liquid—solute water solubilities and molar volumes. Environ Sci Technol. 2005;39:8840–6.
23. Yang K, Wu W, Jing Q, Zhu L. Aqueous adsorption of aniline, phenol, and their substitutes by multi-walled carbon nanotubes. Environ Sci Technol. 2008;42:7931–6.
24. Chiou CT, Peters LJ, Freed VH. A physical concept of soil-water equilibria for nonionic organic compounds. Science. 1979;206:831–2.
25. Kyle BG. Soil-water equilibria for nonionic organic compounds. Science. 1981;213:683.
26. Hung WN, Lin TF, Chiou CT. Solution models for binary components of significantly different molecular sizes. J Solution Chem. 2013;42:1438–51.
27. Wang J, Chen B, Xing B. Wrinkles and folds of activated graphene nanosheets as fast and efficient adsorptive sites for hydrophobic organic contaminants. Environ Sci Technol. 2016;50:3798–808.
28. Yang K, Xing B. Desorption of polycyclic aromatic hydrocarbons from carbon nanomaterials in water. Environ Pollut. 2007;145:529–37.
29. Zhang S, Shao T, Kose HS, Karanfil T. Adsorption of aromatic compounds by carbonaceous adsorbents: a comparative study on granular activated carbon, activated carbon fiber, and carbon nanotubes. Environ Sci Technol. 2010;44:6377–83.
30. Chen W, Duan L, Zhu D. Adsorption of polar and nonpolar organic chemicals to carbon nanotubes. Environ Sci Technol. 2007;41:8295–300.

Publisher's Note